Biophysical Journal Volume 71 July 1996 317–326

Entropy-Driven Instability and Rupture of Fluid Membranes

Julian C. Shillcock and David H. Boal
Department of Physics, Simon Fraser University, Burnaby, British Columbia V5A 1S6 Canada

ABSTRACT A computer simulation is used to investigate hole formation in a model membrane. The model parameters are the stress applied to the membrane, and the edge energy per unit length along the hole boundary (edge tension). Even at zero stress, the membrane has an entropically driven instability against hole formation. Within the model, the minimum edge tension required for the stability of a typical biological membrane is in the region of 1×10^{-11} J/m, which is similar to the edge tension obtained in many measurements of biomembranes. At the zero-stress instability threshold, the hole shape is the same as a self-avoiding ring, but under compression, the hole shape assumes a branched polymer form. In the presence of large holes at zero stress, the membrane itself behaves like a branched polymer. The boundaries of the phase diagram for membrane stability are obtained, and general features of the rate of membrane rupture under stress are investigated. A model in which the entropy of hole formation is proportional to the hole perimeter is used to interpret the simulation results at small stress near the instability threshold.

INTRODUCTION

The isolation of a cell's contents from its surroundings relies upon the mechanical stability of the plasma membrane. The stability of a bilayer against rupture or lysis has been investigated by several experimental means. In electroporation experiments, a membrane subject to an electric field may rupture because of the electrocompressive stress (Harbich and Helfrich, 1979; for recent results, see Glaser et al., 1988; Zhelev and Needham, 1993; Wilhelm et al., 1993; Freeman et al., 1994). The swelling of a cell in a hypoosmotic solution can also lead to membrane rupture (recent work can be found in Ertel et al., 1993; Mui et al., 1993). Many experiments show that the membrane area increases by only 2–3% before rupture, and that the external tension needed to induce rupture is on the order of 10^{-3} to 10^{-2} J/m^2, depending on the chemical composition of the membrane (Evans and Needham, 1987; Needham and Hochmuth, 1989).

Some models of membrane rupture assume that hydrophilic holes are formed in the bilayer through the rearrangement of lipid molecules in a way that keeps their hydrocarbon chains away from the surrounding aqueous medium. Models that have been proposed for membrane rupture include the irreversible opening of a single large hole (Litster, 1975; Wilhelm et al., 1993), the reversible opening of many small holes (Taupin et al., 1975), and several other mechanisms (Abidor et al., 1979; Powell and Weaver, 1986; Popescu et al., 1991). The holes in these models are characterised by an energy per unit length, or edge tension. Model analyses of the experiments typically yield values for the edge tension in the 10^{-11} J/m range (Zhelev and Needham, 1993).

Rupture models have so far neglected the effects of entropy, in the sense that the hole geometry is assumed to minimize the energy, rather than the free energy. For example, Fromherz et al. (Fromherz, 1983; Fromherz et al., 1986) analyzed the topology change between a flat, open sheet and a closed sphere using a zero-temperature model in which the membrane is subject to an edge tension at the perimeter and a bending resistance in the bulk. Based on the maximum radius observed for open membrane sheets after sonication, the edge tension of egg lecithin extracted in this model is 4×10^{-11} J/m.

As can be shown with computer simulations, the stability of model membranes may be temperature dependent (Boal and Rao, 1992b). A spherical membrane conformation that is stable at zero temperature can become unstable at nonzero temperatures for certain combinations of bending resistance and edge tension. The free energy barrier between open and closed membrane topologies is reduced by entropic contributions, which place a lower bound on the edge tension required for membranes to be stable against rupture.

In this paper, we examine membrane stability under stress at nonzero temperatures. We investigate the geometry of a hole during membrane rupture and obtain a phase diagram for the membrane and hole shapes as a function of stress and edge tension. We confirm the bound on the edge tension required for membrane stability that we observed in our three-dimensional studies (Boal and Rao, 1992b). Although the value of the bound depends on the chemical composition of the bilayer, it corresponds to a zero-temperature edge tension of approximately 1×10^{-11} J/m for a typical biomembrane.

In the following section, we review a conventional zero-temperature model for hole formation in two dimensions under stress. Quantitative results for this model at nonzero temperatures are obtained by computer simulations and are presented after the computational techniques are outlined.

Received for publication 14 December 1995 and in final form 15 March 1996.

Address reprint requests to Dr. David H. Boal, Department of Physics, Simon Fraser University, Burnaby, BC V5A 1S6 Canada. Tel.: 604-291-5765; Fax: 604-291-3592; E-mail: boal@sfu.ca.

0006-3495/96/07/317/10 $2.00

The general features of the simulation are consistent with the entropy of hole formation having a linear dependence on the hole perimeter. Results from the simulations are expressed in terms of an elementary length scale a and the inverse temperature β^{-1}. The simulation is of general application, with predictions for specific systems being determined by the choice of a and β. In the final section of the paper, we choose values for these parameters appropriate to biological membranes and summarize the results in physical units.

A brief word on notation: To minimize the number of contexts in which the word "tension" appears, we say that the membrane is subject to a surface stress σ rather than an applied tension. The sign convention is that $\sigma > 0$ corresponds to tension, whereas $\sigma < 0$ corresponds to compression. The surface pressure is related to, but not equal to, the surface stress (see Evans and Waugh, 1977).

MODEL FOR RUPTURE

Our starting point is a commonly used zero-temperature model for membrane rupture involving only two parameters, σ and λ, where σ is the applied surface stress and λ is the edge tension along the hole perimeter at zero temperature (Litster, 1975). In this model, the free energy at zero temperature, F_o, is given by

$$F_o = -\sigma A + \lambda\Gamma. \tag{1}$$

The edge tension, λ, is positive when energy is required to increase the hole perimeter. The area, A, is the total area of the bulk membrane and the hole, and Γ is the perimeter of the hole. At zero temperature, the energy-minimizing shape of the hole is a circle, defined to have radius R. The change in the free energy associated with the formation of a single hole is then

$$\Delta F_o = -\pi R^2\sigma + 2\pi R\lambda. \tag{2}$$

Entropy will contribute to the free energy of Eq. 1 at nonzero temperatures. There are a number of lattice simulations that can be used to estimate the entropy of hole formation, but we delay a discussion of these estimates until after the simulation results are presented.

Holes with $R = 0$ have the lowest free energy for negative stress (compression). However, for positive stress (tension), zero radius holes are only metastable, and R expands without limit in the thermodynamically favored state. At a critical radius R^*, given by

$$R^* = \lambda/\sigma, \tag{3}$$

the free energy barrier against hole formation has a maximum value of

$$\Delta F_o^* = \pi\lambda^2/\sigma. \tag{4}$$

Eq. 4 implies that the barrier against hole formation vanishes only in the $\lambda \to 0$ or $\sigma \to \infty$ limit.

SIMULATION TECHNIQUES

In our simulations, the membrane is treated as a two-dimensional, self-avoiding, tethered manifold consisting of hard spherical beads (vertices) linked together by flexible tethers (bonds). This class of models was originally developed for the study of polymerized membranes (Kantor et al., 1986) and then generalized to simulate fluid membranes of fixed topology by means of an algorithm for tether mobility (Baumgartner and Ho, 1990). Here, we use the Baumgartner/Ho algorithm for fluid membranes and use a bond creation and removal algorithm that allows for topology changes in the fluid membrane (Boal and Rao, 1992b).

The computational membrane is confined to a two-dimensional plane and is subject to periodic boundary conditions. Restricting the membrane to lie in-plane means that our simulation results can be applied to membranes in three dimensions only on length scales that are small compared to the persistence length of the membrane. The persistence length of lipid bilayers is typically greater than a micron, so that our simulation is useful for investigating holes up to perhaps 100 nm in diameter. In fact, the typical hole dimension in cell rupture experiments is thought to be tens of nanometers (Mui et al., 1993), which is well within the applicable range of the simulation.

The boundary and interior of the membrane are defined by bonds and vertices. The number of vertices N is fixed but the number of bonds is not—bonds can be inserted and removed at the membrane boundary. Vertices defining the edge of the membrane are called external, as are bonds linking two external vertices. All other vertices and bonds are internal. Only a single, simply connected hole is allowed in the simulations, although the perimeter of the hole may cross the periodic boundaries.

Eq. 1 forms the basis of the zero-temperature energetics of the simulation. The perimeter Γ is a sum over the lengths of the external bonds, and the area A is the total area of the membrane, including the hole, contained within the periodic boundaries. In addition to Eq. 1, the vertices are subject to step-function potentials that enforce the self-avoidance constraint: the vertices are infinitely repulsive at distances less than the bead diameter a (for all vertex pairs) or greater than $\sqrt{3}\,a$ (for vertex pairs connected by tethers). The maximum tether length could be as large as $2a$ without violating self-avoidance in two dimensions, but $\sqrt{3}\,a$ is chosen so that direct comparison can be made with results from membrane simulations in three dimensions. The average segment length b in the simulations is observed to be $1.34a$, with the difference between the average internal and external segment lengths being less than 1%. Although individual tethers do not have a fixed length, fluctuations in the bulk membrane area around its mean are small.

A set of appropriately weighted sample configurations is generated using the usual Metropolis Monte Carlo technique in which trial moves are made on the vertex positions and connectivity. A sweep across the membrane involves the following steps: 1) An attempt is made to change the

position of each vertex by choosing a new position randomly from within a square box of length $2l$ to the side centered on the old position. 2) An attempt is made to reconnect every internal bond. Each internal bond is defined by its two end vertices v_1 and v_2, and its two "opposite" vertices v_a and v_b. The move consists of reconnecting the bond to v_a and v_b, with v_1 and v_2 becoming the new "opposite" vertices. 3) An attempt is made to remove each external bond, reducing the total number of bonds by one while converting two internal bonds into external bonds. 4) An attempt is made to convert each external vertex into an internal vertex by adding a new external bond directly between the two external nearest neighbors of the vertex. The simulation forbids the total number of external bonds from decreasing below four, so that a single hole, however tiny, is always present in the membrane.

Rectangular periodic boundary conditions are imposed by connecting the configuration to its periodic images, translated by the side lengths L_x and L_y of the boundary box in the x and y directions, respectively. In addition to the vertex and bond moves 1) through 4), attempts are made to rescale L_x and L_y independently. Simultaneously, the vertex positions are rescaled proportionately to the change in L_x and L_y. The periodic box rescaling algorithm for the isobaric ensemble was developed by Wood (1968) and is described in more detail elsewhere (Hansen and McDonald, 1986). All trial moves on positions, connectivities, and boundaries are accepted or rejected according to the Boltzmann weight, $\exp(-\beta\Delta F_o)$.

An ensemble of configurations generated by this technique is an appropriate sample of the system at finite temperature. The simulation is used to investigate the static properties of membranes, such as mean areas and elastic moduli, as well as dynamic properties, such as the mean time for rupture under tension. For static properties, 400-1000 sample configurations are generated at each (σ,λ) combination. Each configuration is separated by a time $\tau = N/l^2$ Monte Carlo sweeps, where we use $l = 0.1$. Before sample collection, each initialization is allowed to relax for 10τ. For dynamic properties, such as the rupture rate, a configuration first is allowed to relax at the chosen stress with bond removal forbidden, and then the time evolution of the configuration is followed after $\beta\lambda a$ is set and bond insertion and removal are permitted. Rupture rates are calculated using 400 initializations for each (σ,λ) combination.

The membrane in-plane elastic constants reported here are determined from fluctuations in the periodic box lengths. For example, the compression modulus K_A is given by

$$\beta K_A = \langle A\rangle/(\langle A^2\rangle - \langle A\rangle^2), \tag{5}$$

where $A = L_xL_y$ and $\langle \ldots \rangle$ indicates an ensemble average. Because the shear and Young's moduli vanish for the fluid membranes investigated in this paper, only the compression modulus is displayed in the following sections.

SIMULATION RESULTS

The simulations allow the determination of the membrane and hole geometry, the system elasticity, and the rupture rate under stress. Several of these quantities, particularly the geometry, depend on the edge tension and applied stress in nontrivial ways. To simplify the presentation, we group the results into three categories according to the applied stress: specifically, stress-free, compressed networks, and stretched networks.

Networks at zero stress

Stress-free networks are governed by one independent variable, namely the edge tension, in the dimensionless combination $\beta\lambda a$. A snapshot of a typical membrane configuration at zero stress and $\beta\lambda a = 1.23$ is shown in Fig. 1. The obvious membrane hole shown in the figure is simply connected, even though the hole perimeter passes across the periodic boundaries. One can see that the vertices are approximately sixfold coordinated on average, although many five- and sevenfold coordinated vertices are present. The variable connectivity results from the bond mobility algorithm that is used here for fluid membranes.

Only relatively small holes are present if $\beta\lambda a > 1.3$, whereas large holes are observed for $\beta\lambda a < 1.2$. The hole size changes rapidly around $\beta\lambda a = 1.24$, as illustrated in Fig. 2, where the reduced perimeter Γ/Na of the hole is plotted against the edge tension for a number of system sizes. Below $\beta\lambda a = 1.0$, the holes approach the maximum value allowed by the system size N. We denote the transition value of the edge tension at zero stress as λ^*, with $\beta\lambda^* a = 1.24$. Alternatively, if we define the average segment length as b ($b = 1.34a$), then the transition occurs at $\beta\lambda^* b = 1.66$.

The appearance of a hole in the membrane allows the membrane/hole system to undergo large area fluctuations, corresponding to a small compression modulus. The behavior of the compression modulus K_A, as extracted from the simulations using Eq. 5, is shown in Fig. 3. At zero stress, the modulus is close to zero for $\beta\lambda a < 1.2$ and is close to

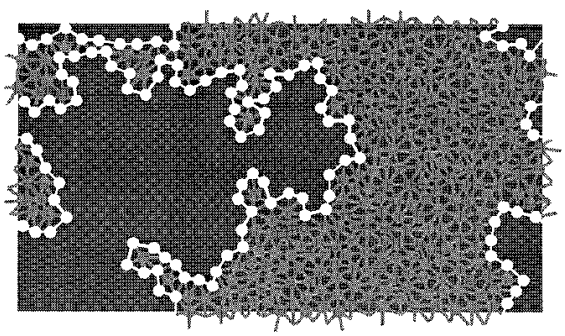

FIGURE 1 Snapshot of a configuration with $N = 400$ vertices at zero stress. The edge tension is $\beta\lambda a = 1.23$.

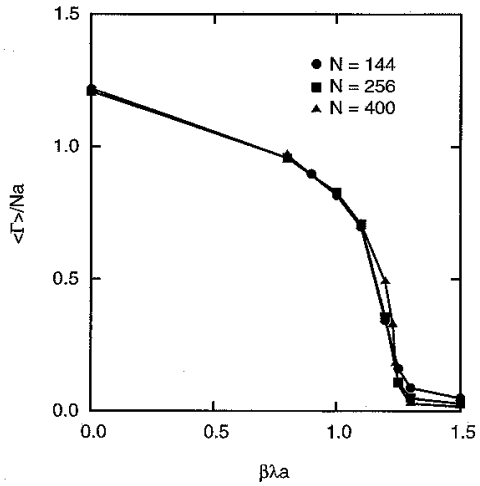

FIGURE 2 Reduced hole perimeter $\langle\Gamma\rangle/Na$ shown as a function of edge tension $\beta\lambda a$ for system sizes N = 144, 256, and 400. The edge tension at the transition is estimated to be $\beta\lambda^* a$ = 1.24.

the pure fluid modulus, $\beta K_A a^2$ = 18 (Boal, 1993), for $\beta\lambda a > 1.4$. The range of edge tension over which the change in K_A occurs is similar to that observed for the change in the hole perimeter, although the change in the modulus is not as abrupt as it is in the hole perimeter. The hole has no effect on the shear modulus, which is always zero for a fluid membrane.

Membrane geometry

Fig. 2 demonstrates that the average hole perimeter scales linearly with the number of vertices N in the membrane.

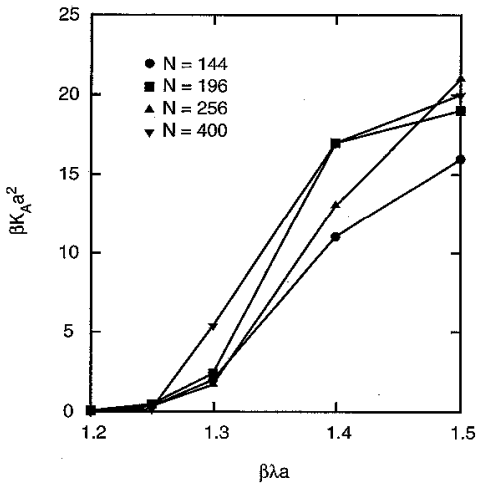

FIGURE 3 Dimensionless compression modulus $\beta K_A a^2$ of the membrane/hole system as a function of edge tension $\beta\lambda a$ for system masses N = 144, 196, 256, and 400.

Such scaling behavior reflects the branched polymer scaling of the membrane itself, a result found previously for fluid membranes in three dimensions (Boal and Rao, 1992b). For branched polymers confined to two dimensions, the ensemble averages of the perimeter Γ and the radius of gyration R_g^2 scale with the mass M of the object like

$$\langle\Gamma\rangle = \Gamma_o M^{1.0} \tag{6a}$$

$$\langle R_g^2\rangle = R_o^2 M^{1.28}, \tag{6b}$$

where Γ_o and R_o^2 are proportionality constants that are independent of M for large systems (Derrida and Stauffer, 1985).

The branched polymer scaling of the membrane can be seen more clearly if the average hole perimeter is plotted against the average membrane area at fixed edge tension. As Fig. 4 illustrates, the average hole perimeter is small even for an edge tension of $\beta\lambda a$ = 1.3, which is just above the transition value. For edge tensions below the instability point, the average hole perimeter clearly scales as a power of the membrane area in the figure. Power law fits to the data in Fig. 4 give exponents δ of 1.0, 1.0, and 1.4 ± 0.15 at $\beta\lambda a$ = 0.8, 1.0, and 1.2, respectively, for the analog of Eq. 6a, $\langle\Gamma\rangle = \Gamma_o N^\delta$. Data near $\beta\lambda^* a$ have relatively large uncertainties and potentially strong finite size effects; we were unable to extract the membrane scaling behavior at the transition.

Hole geometry

On large enough length scales all fluid membranes in three dimensions are expected to show branched polymer scaling in both open and closed geometries (Gompper and Kroll,

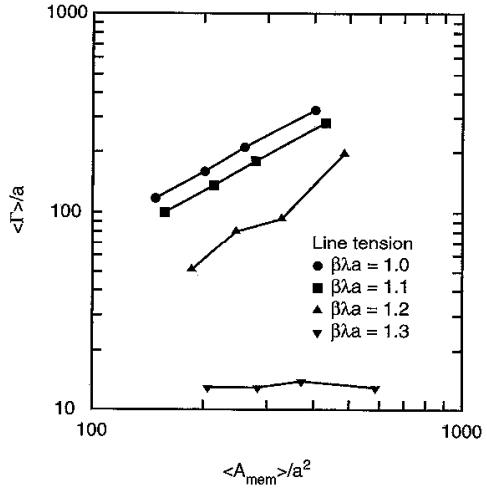

FIGURE 4 Average hole perimeter $\langle\Gamma\rangle/a$ plotted against average membrane area $\langle A_{mem}\rangle/a^2$ for zero stress and edge tensions $\beta\lambda a$ = 1.0, 1.1, 1.2, and 1.3. Each data point is determined at a fixed value of N: 144, 196, 256, and 400.

1992; Boal and Rao, 1992a). Here, we have shown that fluid membranes in two dimensions behave like branched polymers if the edge tension is sufficiently small. We now investigate the properties of the membrane hole (as opposed to the bulk membrane area or radius of gyration), an object that has a poorly defined area in three dimensions.

The scaling behavior of the holes is difficult to determine for $\beta\lambda a > 1.3$, because most holes are close to the minimum size allowed by the simulation algorithm. Near the transition region, the holes have a broader size distribution, and it is possible to perform a scaling analysis. We find no simple functional relationship between the membrane size and the area or radius of gyration of the hole at the transition $\beta\lambda^* a$. There is a relationship between the membrane area and hole perimeter, as we have discussed, but we interpret this relationship as one between the membrane perimeter and the membrane mass.

However, a simple functional relationship is found between the average hole area $\langle A_h \rangle$ and the hole perimeter $\langle \Gamma \rangle$ near the transition $\beta\lambda^* a$. This is shown in Fig. 5, in which the area and perimeter are normalized by the average segment or bond length b of the hole boundary. At the transition value $\beta\lambda^* a$, the area and the radius of gyration scale like $n^{3/2}$. Both of these scaling relationships are expected for a self-avoiding ring, or SAR (Leibler et al., 1987):

$$\langle A \rangle = A_0 n^{3/2} \tag{7a}$$

$$\langle R_g^2 \rangle = R_0^2 n^{3/2}. \tag{7b}$$

The prefactor A_0 in Eq. 7a is $0.16b^2$ for the interparticle potential used in the simulation. The equivalence between the self-avoiding ring and the hole in the membrane/hole system can be seen in the curves marked by upright and inverted solid triangles in Fig. 5. The figure also shows the area expected for circular holes, which clearly are larger than the holes observed in the simulation. This result is not really surprising, and emphasizes that circular holes dominate the free energy only for temperatures $k_B T \ll (\lambda a)^{-1}$.

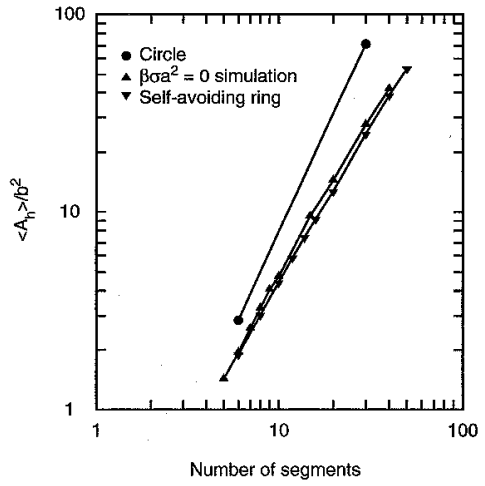

FIGURE 5 Average hole area $\langle A_h \rangle / b^2$ for a fixed number of segments n shown as a function of the number of segments. The area has been normalized by the average segment length $b = \langle \Gamma \rangle / n$, where the expectation is over holes with a fixed number of segments (that is, the expectation is not over all n simultaneously). The parameters are $\beta\lambda a = 1.25$ and $\beta\sigma a^2 = 0$. The areas expected for a circle and a self-avoiding ring are shown for comparison.

Membranes under compression

There are examples of quasi-two-dimensional networks embedded in three dimensions in which a compressive stress can be placed on the network without it buckling into the third dimension. Because our model uses a triangulated network to represent a continuum membrane, the simulation results could be applied to a class of quasi-two-dimensional networks under compression. Although we do not undertake such applications in this paper, we report the elastic properties and phase diagram for membranes under small compressive stress.

From Eq. 1, the area of the membrane/hole system under compression ($\sigma < 0$) should be less than the corresponding value at zero stress. The motion of the network elements is restricted at high density, resulting in a large compression modulus, as shown in Fig. 6. All values for $\beta\lambda a$ selected for the figure correspond to unstable membranes at $\sigma = 0$. The compression moduli are seen to increase steadily with compressive stress and rise significantly beyond $\beta K_A a^2 = 18$, which is the value for our pure computational fluid membrane at zero stress. Furthermore, the figure shows that $\beta K_A a^2$ does not necessarily rise immediately to 18 for any compressive stress. The membrane area exhibits considerable elasticity at small applied stress away from the transi-

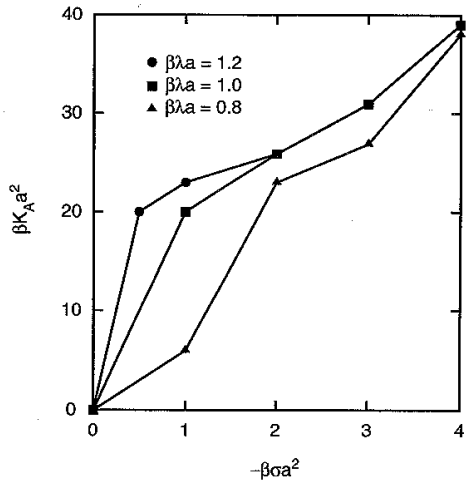

FIGURE 6 Dimensionless area compression modulus $\beta K_A a^2$ as a function of applied stress for three values of the edge tension $\beta\lambda a = 0.8$, 1.0, and 1.2. The moduli are determined from a system with $N = 196$ vertices.

tion region (e.g., $\beta\lambda a = 0.8$), indicating that a population of holes is present.

Naturally, the holes are smaller in compressed systems than they are at zero stress, for a given $\beta\lambda a$. Furthermore, the holes may belong to a different class of shapes. Leibler et al. (1987) found that polymer rings at zero stress scale like self-avoiding walks, whereas rings under compression scale like branched polymers. We have obtained the scaling exponents for hole area and radius of gyration as a function of hole perimeter for several parameter combinations at $\sigma < 0$ (compression), and the exponents are consistent with branched polymer scaling. For example, averaged over several membrane masses, the holes in the simulation are described by

$$\langle A\rangle/a^2 = 0.56n^{(1.05 \pm 0.01)} \tag{8a}$$

$$\langle R_g^2\rangle/a^2 = 0.17n^{(1.2 \pm 0.1)} \tag{8b}$$

at $\beta\lambda a = 0.8$ and $\beta\sigma a^2 = -1.0$, where n is the number of segments in the hole boundary. This scaling behavior agrees with the branched polymer scaling displayed in Eq. 6.

Mapping out the complete phase diagram by simulation is a task beyond our computational capabilities. For each ($\beta\sigma a^2$, $\beta\lambda a$) combination, the scaling exponents must be determined by a power law fit to a geometric quantity as a function of N, a task that is computationally demanding. We present only a survey of the phase diagram at negative stress in Fig. 7. The labels for the scaling of the hole and/or membrane in the figure are largely self-explanatory. In the "closed" region, only very small holes are present in any appreciable abundance. In all other regions, holes that span the system are present. The phase boundary between open and closed configurations has a steep slope as a function of the edge tension if $\beta\lambda a < 1$. The straight line passing through $\beta\lambda^* a$ is the phase boundary expected if the entropy of hole formation depends linearly on n, as explained in a later section. As observed in the previous section on membranes at zero stress, Fig. 7 demonstrates that the holes present in the model membrane are not circular at high temperatures.

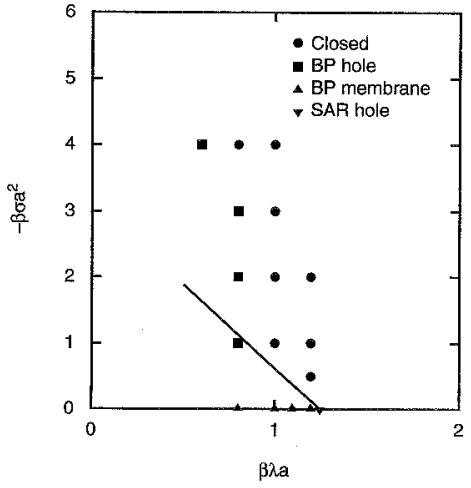

FIGURE 7 Instability regions for spontaneous hole formation under compression ($\sigma < 0$). Unstable regions are labeled by the hole or membrane geometry (SAR = self-avoiding ring, BP = branched polymer), and the stable regions are referred to as closed. The approximate phase boundary given by Eq. 13 is indicated by the straight line.

Membranes under tension

The thermodynamically favored state for membranes under tension ($\sigma > 0$) is the ruptured state with at least one large hole. This is a reflection of Eq. 1, in which the area term, which lowers the free energy, grows as the hole radius squared, whereas the edge tension term, which raises the free energy, grows only as the hole radius. However, there may be a barrier against hole growth, and Eqs. 3 and 4 give the hole radius and barrier free energy expected for circular holes at zero temperature. The free energy barrier against hole formation at high temperatures may be different from Eq. 4 if the holes are not circular.

The simulation model can be used to investigate the barrier against rupture under tension. To establish an approximate definition of the computational rupture point, we follow the time evolution of 20 configurations for approximately 1 million Monte Carlo sweeps each. The hole in each configuration is observed to oscillate in perimeter up to about $n = 10$ to 12 segments, but almost all holes that reach a size of 20 segments grow irreversibly. We define the rupture point as that time when the hole first has 20 segments along its boundary.

Each initialization in the sample is allowed to relax according to a procedure described earlier in this paper, after which the time to rupture is measured in Monte Carlo sweeps. These times are collected to form a distribution, $D(t)$. Each distribution is approximately exponential and can be fitted with a functional form

$$D(t) = D(0)\exp(-\rho t). \tag{9}$$

where ρ is the rupture rate. If the distribution is exponential over its entire range, then we expect $\rho^{-1} = \langle t\rangle$. This equality is found to be obeyed within the statistical accuracy of the simulation for all parameter combinations investigated. Given that $\langle t\rangle$ can be obtained with greater accuracy than ρ for fixed sample size, the rates quoted in the remainder of this paper are, in fact, $\langle t\rangle^{-1}$.

The general features of membrane rupture in the model are demonstrated by Fig. 8:

1. For fixed stress, the rupture rate decreases with increasing edge tension.

2. For fixed edge tension, the rupture rate increases with applied stress.

Although these qualitative characteristics are expected from the barrier height against hole growth given by Eq. 4, note that this equation predicts that small holes should be

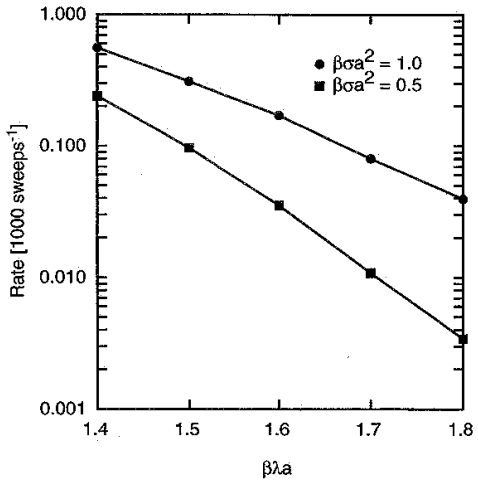

FIGURE 8 Rupture rates as a function of edge tension at two values of the applied surface stress: $\beta\sigma a^2 = 0.5$ and 1.0. The rate shown here is $\langle t \rangle^{-1}$; see text after Eq. 9 for discussion.

metastable for all values of the edge tension, whereas we find that systems are unstable if their edge tension is less than a stress-dependent threshold value.

We are unable to determine the scaling characteristics of the holes during rupture. Plots of hole area against hole perimeter do not show any specific scaling form across the barrier region of $10 < n < 20$. Inspection of the hole configurations only shows that they are larger in area than self-avoiding rings but smaller than full circles.

DISCUSSION

A schematic phase diagram that summarizes the geometrical properties of our membrane/hole model is shown in Fig. 9. The geometry of the holes can be categorized according to at least three generic descriptions:

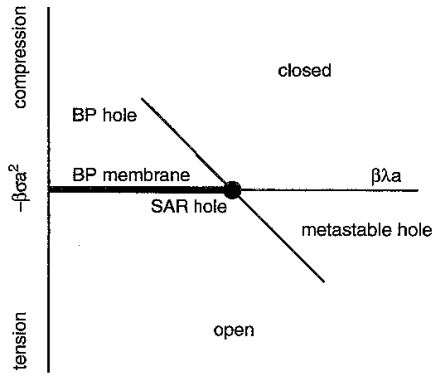

FIGURE 9 Schematic phase diagram for the model membrane/hole system.

1. Large holes are present for a range of edge tensions at both positive and negative stress. In some regions, open holes may show the same scaling as branched polymers ($\sigma < 0$) or self-avoiding rings ($\lambda = \lambda^*$, $\sigma = 0$). In other regions, large holes may not possess well-defined scaling; these regions include positive stress (tension) and $\lambda < \lambda^*$ at $\sigma = 0$.

2. Small holes are observed under compression and edge tensions larger than a stress-dependent transition value.

3. Small metastable holes may be present for positive stress and edge tensions greater than a stress-dependent transition value.

In this section, the region near λ^* is discussed in more detail; we interpret the results using a simple model for the free energy, and we apply the results to biomembranes.

Free energy of hole formation

At nonzero temperatures, an entropic contribution $-TS$ must be added to Eq. 1 for the free energy. This contribution must include the restricted vertex movement in the bulk membrane and on the membrane boundary. It must also reflect the larger configuration space available to a network with a hole present.

As a simple model, we make the possibly dramatic assumption that the entropy difference between networks with and without holes is dominated by the entropy associated with the hole boundary. We regard the membrane hole boundary as a closed self-avoiding path of n steps of constant length b. The number of configurations of such paths, $\Omega(n)$, has been investigated in both two and three dimensions for several classes of paths on a lattice, including branched polymers and self-avoiding rings (McKenzie, 1976; Glaus, 1988), and has the general form

$$\Omega(n) = \Omega_o z^n n^{\alpha-2} \tag{10}$$

where z is the connectivity constant of the lattice (and has a value somewhat less than the coordination number), α is an exponent, and Ω_o is a prefactor that is independent of n. The entropic contribution to the free energy, $k_B T \ln \Omega$, is then proportional to n to leading order for the configurations obeying Eq. 10.

The lattice results suggest that the entropy for hole formation grows linearly with n, with a corresponding free energy difference of

$$\Delta F = -\sigma A + \lambda b n - k_B T C n. \tag{11}$$

where C is a constant. Equation 11 predicts that the hole shape should be circular at low temperature (large $\beta\lambda b$) and highly convoluted at high temperature (small $\beta\lambda b$). Thus, even when there is no external stress, the membrane is unstable against the formation of highly convoluted holes if $\beta\lambda b < C$. The simulations fix $C = \beta\lambda^* b = 1.66$. Using $z = 4.15$ for a self-avoiding walk (McKenzie, 1976), Eq. 10 predicts $\beta\lambda^* b = 1.4$, which is fortuitously close to the observed value. An argument similar to this has been used

to interpret the instability of fluid membranes against entropically driven hole formation in three dimensions (Boal and Rao, 1992b).

Equation 11 can be used to estimate the phase boundary near the zero-stress transition for systems under compression in which the holes have the form of branched polymers. The change in free energy associated with the formation of branched polymer holes is proportional to n, because the hole area is proportional to the hole perimeter. Specifically, the change in free energy per segment is

$$\Delta\beta F/n = -0.56\beta\sigma a^2 + 1.34\beta\lambda a - 1.66. \quad (12)$$

Because it takes no free energy to create a new hole segment at the transition, we expect that the transition stress σ_t should be related to the transition edge tension λ_t via

$$\beta\sigma_t a^2 = 2.5\beta\lambda_t a - 3.1. \quad (13)$$

As shown in Fig. 7, the phase boundary predicted by Eq. 13 is not in qualitative disagreement with the known phase behavior.

At $T > 0$, the free energy barrier against hole formation under tension may vanish. Assuming that the holes formed under tension are approximately self-avoiding rings (see Eq. 7), then the free energy reduction from the stress term will be $-0.16\beta\sigma b^2 n^{3/2}$ (σ is positive) and the barrier against the formation of SAR holes is

$$\Delta\beta F_{SAR} = -0.16\beta\sigma b^2 n^{3/2} + \beta\lambda n b - 1.66n. \quad (14)$$

For a given (σ, λ) combination, the free energy of Eq. 14 increases with n until it reaches a maximum at a hole with segment number n^*_{SAR}, given by

$$n^*_{SAR} = 4 \cdot (\beta\lambda b - 1.66)^2/9 \cdot (-0.16\beta\sigma b^2)^2 \quad (15)$$

at which the barrier height, $\Delta\beta F^*_{SAR}$, is

$$\Delta\beta F^*_{SAR} = 4 \cdot (\beta\lambda b - 1.66)^3/27 \cdot (-0.16\beta\sigma b^2)^2 \quad (16)$$

Numerical evaluation of Eqs. 4 and 16 demonstrates that SAR holes may have a substantially lower barrier against growth than do circular holes, depending on stress and edge tension.

In the theory of thermally induced reactions, the reaction rate depends most strongly on the reaction free energy as $\exp(-\Delta\beta F^*)$. Assuming that

$$\rho(\sigma, \lambda) = \rho(\sigma)\exp(-\Delta\beta F^*), \quad (17)$$

where $\rho(\sigma)$ is a stress-dependent normalization constant, the functional forms of Eqs. 4 and 16 can be compared to the simulation data. Both of these forms, normalized to the simulation data at $\beta\sigma a^2 = 1$ and $\beta\lambda a = 1.6$, are shown in Fig. 10. The rates found in the simulation lie at a point intermediate between the SAR and circular hole predictions, even if the holes ultimately become circular once the system has crossed the barrier.

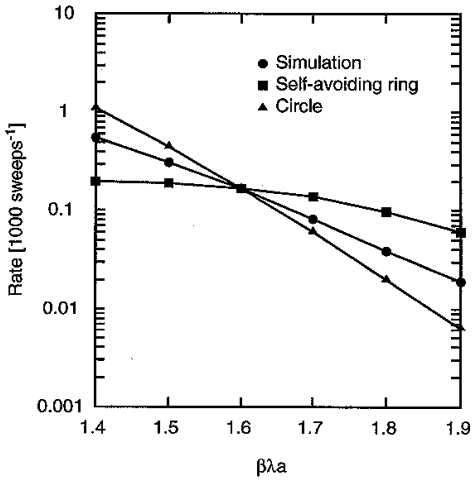

FIGURE 10 Rupture rates found by simulation as a function of edge tension $\beta\lambda a$ for fixed stress $\beta\sigma a^2 = 1$. The system has $N = 144$ vertices. Shown for comparison are the trends expected for rupture via holes shaped like circles or self-avoiding rings. See text for an explanation of the comparisons.

Application to lipid bilayers

The motivation for this work is the investigation of the mechanical stability of biological membranes under stress. The simulation results can be applied to biomembranes or other systems once the temperature and length scales are assigned physical values. We choose room temperature to fix β. The length scale is system dependent, and what we wish to do here is obtain the features of a "typical" membrane. Two means of setting the length scale are:

1. Equate the average membrane area per vertex, $\sqrt{3}b^2/2$, with the average area per lipid of about 0.5 nm^2.

2. Equate the compression modulus of the bulk computational membrane, which is $\beta K_A b^2 = 32$, with a typical bilayer compression modulus of about 0.3 J/m^2.

Methods 1 and 2 yield $b = 0.76$ nm and 0.65 nm, respectively. We choose $b = 0.7$ nm as representative of the biomembrane length scale.

The physical value of the stability bound at $\beta\lambda^* b = 1.66$ corresponds to an edge tension λ^* of 9×10^{-12} J/m using representative values of β and b. The bound is membrane-specific because λ^* is a function of the length scale b. Although this bound is close to the edge tensions extracted in model-dependent analysis of rupture data, it does not imply that biomembranes are almost unstable. The methodology for obtaining the edge tension experimentally usually involves a zero-temperature model for rupture that relates the measured quantity, such as the applied stress at rupture, to the model quantity—the edge tension. The models of which we are aware do not include temperature-dependent corrections. Thus, the fact that the quoted values for the edge tension range from 1×10^{-11} to 4×10^{-11} J should be taken as evidence that biomembranes have edge tensions

that are probably several times the minimum required for stability.

We now turn to the rupture dynamics predicted by the simulations. Lysis tensions are commonly observed to be in the region of 6×10^{-3} J/m^2, which is about 1/20 of the bilayer compression modulus. In simulation units, such tensions correspond to $\beta\sigma b^2 = 0.7$. Thus, the typical edge tension and lysis tension found experimentally are in the range studied by the simulation. We have demonstrated that entropy plays an important role in the rupture reaction mechanism for simulations in this parameter range and may lower the barrier against rupture significantly below the $5\text{–}70k_BT$ (for $\lambda = 1\text{–}4 \times 10^{-11}$ J and $\sigma = 6 \times 10^{-3}$ J/m^2) predicted for a circular hole.

SUMMARY

We have obtained a phase diagram for the static properties of a model fluid membrane that is under stress and characterized by a single hole with a zero-temperature edge tension parameter λ. At zero stress and large edge tension, the membrane possesses small holes consistent with statistical fluctuations. However, the membrane becomes unstable against hole growth for edge tensions less than $\beta\lambda^* a = 1.24$. At the transition point, the holes scale like self-avoiding rings. For edge tensions smaller than the transition value, the holes at zero stress do not show any particular scaling behavior, whereas the bulk membrane scales like a branched polymer. The instability at zero stress is similar to the instability of fluid membranes embedded in three dimensions, although the transition value in three dimensions ($\beta\lambda^* a = 1.0$; Boal and Rao, 1992b) is somewhat smaller than in two dimensions. Even when the networks are compressed, they may be unstable against hole formation, although the value of λ at the instability threshold is both stress dependent and smaller than the corresponding value at zero stress. In the instability region at $\sigma < 0$ (compression), holes exhibit branched polymer scaling. At $\sigma > 0$ (tension), large holes are thermodynamically favored. However, there may be a free energy barrier against the formation of such holes, with the barrier growing as a power law function of the edge tension.

If the entropy change associated with hole formation is dominated by the configurational entropy of the hole shape, then lattice results argue that the free energy change is proportional to the hole perimeter. This assumption leads to quantitative predictions for the phase boundary near the zero stress transition and for the rupture rates of stretched membranes. However, the predictions are only in rough agreement with the simulation results.

We have estimated the energy and length scales in our model that correspond to a typical lipid bilayer. The zero-temperature edge tension is found to be 9×10^{-12} J/m. This value is in the same region as the edge tensions obtained from model-dependent analyses of experiments. Most models extract a quantity that corresponds to $\lambda - TS/b$ in the simulations, that is, the zero-temperature edge tension reduced by the entropic contribution arising from hole formation. Hence, the quoted values are an underestimate of our parameter λ, although whether they are a significant underestimate remains to be seen. Measured values of the edge tension appear to be larger than the lower bound for stability λ^* obtained here.

Now, there are several features of membrane rupture that have been omitted in the simulation. We have not included an activation energy for the formation of a hole, and we have allowed only a single hole in the membrane; it may be that many holes in the membrane act collectively. Curvature dependence of the edge tension has been omitted as well. For example, it may be that the edge energy of the lipid surface at the hole boundary depends on the mean curvature of the surface at the hole boundary, so that straight boundaries have larger edge tensions than curved boundaries with small or zero mean curvature. Molecular-level calculations should indicate the importance of boundary curvature effects and the degree to which the model must be revised or extended.

The authors wish to thank Evan Evans, Ross Hallett, Bernie Nickel, Janet Wood, and Michael Wortis for many stimulating discussions.

This work is supported in part by the Natural Sciences and Engineering Research Council of Canada.

REFERENCES

Abidor, I. G., V. B. Arakelyan, L. V. Chernomordik, Y. A. Chizmadzhev, V. F. Pastushenko, and M. R. Tarasevich. 1979. Electric breakdown of bilayer lipid membranes. I. The main experimental facts and their qualitative discussion. *Bioelectrochem. Bioenerg.* 6:37–52.

Baumgartner, A., and J.-S. Ho. 1990. Crumpling of fluid vesicles. *Phys. Rev. A.* 41:5747–5750.

Boal, D. H. 1993. Rigidity and connectivity percolation in heterogeneous polymer-fluid networks. *Phys. Rev. E.* 47:4604–4606.

Boal, D. H., and M. Rao. 1992a. Scaling behavior of membranes in three dimensions. *Phys. Rev. A.* 45:R6947–R6950.

Boal, D. H., and M. Rao. 1992b. Topology changes in fluid membranes. *Phys. Rev. A.* 46:3037–3045.

Derrida, B., and D. Stauffer. 1985. Corrections to scaling and phenomenological renormalization for 2-dimensional percolation and lattice animal problems. *J. Physiol.* 46:1623–1630.

Ertel, A., G. Marangoni, J. Marsh, F. R. Hallett, and J. M. Wood. 1993. Mechanical properties of vesicles. I. Coordinated analysis of osmotic swelling and lysis. *Biophys. J.* 64:426–434.

Evans, E. A., and D. Needham. 1987. Physical properties of surfactant bilayer membranes: thermal transitions, elasticity, rigidity, cohesion and colloidal interactions. *J. Phys. Chem.* 91:4219–4228.

Evans, E. A., and R. Waugh. 1977. Mechano-chemistry of closed, vesicular membrane systems. *J. Coll. Interface Sci.* 60:286–298.

Freeman, S. A., M. A. Wang, and J. C. Weaver. 1994. Theory of electroporation of planar bilayer membranes: predictions of the aqueous area, change in capacitance and pore-pore separation. *Biophys. J.* 67:42–56.

Fromherz, P. 1983. Lipid-vesicle structure: size control by edge-active agents. *Chem. Phys. Lett.* 94:259–266.

Fromherz, P., C. Röcker, and D. Rüppel. 1986. From discoid micelles to spherical vesicles: the concept of edge activity. *Faraday Discuss. Chem. Soc.* 81:39–48.

Glaser, R. W., S. L. Leikin, L. V. Chernomordik, V. F. Pastushenko, and A. I. Sokirko. 1988. Reversible electrical breakdown of lipid bilayers: formation and evolution of pores. *Biochim. Biophys. Acta.* 940:275–287.

Glaus, U. 1988. Monte Carlo study of self-avoiding surfaces. *J. Stat. Phys.* 50:1141–1166.

Gompper, G., and D. M. Kroll. 1992. Shape of inflated vesicles. *Phys. Rev. A.* 46:7466–7473.

Hansen, J. P., and I. R. McDonald. 1986. Theory of Simple Liquids. Oxford University Press, New York.

Harbich, W., and W. Helfrich. 1979. Alignment and opening of giant lecithin vesicles by electric fields. *Z. Naturforsch.* 34A:1063–1065.

Kantor, Y., M. Kardar, and D. R. Nelson. 1986. Statistical mechanics of tethered surfaces. *Phys. Rev. Lett.* 57:791–794.

Leibler, S., R. R. P. Singh, and M. E. Fisher. 1987. Thermodynamic behavior of two-dimensional vesicles. *Phys. Rev. Lett.* 59:1989–1992.

Litster, J. D. 1975. Stability of lipid bilayers and red blood cell membranes. *Phys. Lett. A.* 53:193–194.

McKenzie, D. S. 1976. Polymers and scaling. *Physics Rep.* 27:35–88.

Mui, B. L.-S., P. R. Cullis, E. A. Evans, and T. D. Madden. 1993. Osmotic properties of large unilamellar vesicles prepared by extrusion. *Biophys. J.* 64:443–453.

Needham, D., and R. M. Hochmuth. 1989. Electro-mechanical permeabilisation of lipid vesicles. *Biophys. J.* 55:1001–1009.

Popescu, D., C. Rucareanu, and Gh. Victor. 1991. A model for the appearance of statistical pores in membranes due to self-oscillations. *Bioelectrochem. Bioenerg.* 25:91–103.

Powell, K. T., and J. C. Weaver. 1986. Transient aqueous pores in bilayer membranes: a statistical theory. *Bioelectrochem. Bioenerg.* 15:211–227.

Taupin, C., M. Dvolaitzky, and C. Sauterey. 1975. Osmotic pressure induced pores in phospholipid vesicles. *Biochemistry.* 14:4771–4775.

Wilhelm, C. M., M. Winterhalter, U. Zimmermann, and R. Benz. 1993. Kinetics of pore size during irreversible electrical breakdown of lipid bilayer membranes. *Biophys. J.* 64:121–128.

Wood, W. W. 1968. Monte Carlo calculations for hard disks in the isothermal-isobaric ensemble. *J. Chem. Phys.* 48:415–434.

Zhelev, D. V., and D. Needham. 1993. Tension stabilized pores in giant vesicles: determination of pore size and pore line tension. *Biochim. Biophys. Acta.* 1147:89–104.